12,05

Structural and magnetic properties of $Co_{1-x}Zn_xFe_2O_4$ ($0 \leq x \leq 1$) nanoparticles for biomedical applications

© A.S. Kamzin[1], V.G. Semenov[2], L.S. Kamzina[1]

[1] Ioffe Institute,
St. Petersburg, Russia
[2] St. Petersburg State University,
St. Petersburg, Russia

E-mail: ASKam@mail.ioffe.ru

Received March 5, 2024
Revised March 5, 2024
Accepted March 6, 2024

Magnetic nanoparticles of Zn-substituted $CoFe_2O_4$ spinel ferrites $Co_{1-x}Zn_xFe_2O_4$ (at $x = 0.0$, 0.2, 0.4, 0.6, 0.8, 1.0) were successfully synthesized by chemical co-precipitation. The structural, morphological and magnetic properties of the obtained particles were studied and characterized by X-ray diffraction (XRD), vibrating-sample magnetometry (VSM), Raman and Mössbauer spectroscopy. The introduction of zinc ions causes noticeable changes in the structural and magnetic properties of spinel ferrite. The sizes of particles of $Co_{1-x}Zn_xFe_2O_4$ change from 10 to 3 nm with an increase of the number of Zn ions according to X-ray data and their sizes change from 15 to 4 nm according to Mössbauer data. It was found that the saturation magnetization increases with an increase of the amount of Zn to $x = 0.4$ and gradually decreases with a further increase of the concentration of Zn. The important information about the difference between the magnetic structures of the surface layer and the volume of particles was obtained for the first time using Mössbauer spectroscopy without external magnetic fields. A collinear ordering of spin moments is observed in the volume of magnetic nanoparticles of ferrite $Co_{1-x}Zn_xFe_2O_4$, whereas a canting spin structure is observed on the surface of particles because of the impact of the surface. The mechanism of transition of spinel ferrite MNPs from a magnetically ordered to a paramagnetic state with the introduction of paramagnetic ions is described. Studies have shown that the obtained nanoparticles are perspective in view of biomedical applications.

Keywords: spinel ferrites, magnetic structure, superparamagnetism, Mössbauer spectroscopy, materials for biomedicine.

DOI: 10.61011/PSS.2024.04.58207.44

1. Introduction

The unique character and complexity of predicting the properties of magnetic fluids (MF), created in 1960 for NASA space programs, resulted in the active development of fundamental studies of MF for practical application [1–3]. MF are colloidal systems consisting of magnetic micron or nanoscale particles dispersed into a carrier liquid [3,4]. MNPs are evenly distributed by thermal motion in the carrier fluid due to their small size and react to the magnetic field as a whole. Currently, MFs are used as magnetic-liquid high-vacuum seals; tilt angle sensors, magnetic separators, acoustic speakers, shock absorbers and dampers, water purifiers from petroleum products. Biomedicine is the most important application of MF, namely: targeted drug delivery [5,6], contrast enhancement of magnetic tomography and X-ray diagnostics, magnetic hyperthermic therapy (MHT) of malignant tumors [7,8].

Antitumor drugs are harmful to a living organism, therefore they are mixed with a magnetic liquid and injected into the blood, then the resulting mixture is concentrated at the affected area using an external magnet, thus causing no harm to the body. Magnetic nanoscale particles (MNPs) introduced with the MF into the organ affected by a malignant tumor are heated to temperatures of 43−46° when an alternating magnetic field is applied and their heat destroys malignant cells without damaging healthy ones [7,8]. MHT cancer treatment does not require surgical intervention, and does not affect other organs being a local treatment, since there are no MNP in them.

The properties and applications of a MF are determined by the complex characteristics of its components (magnetic particles, dispersion medium and stabilizer). MNCs are the main component of MF, forming its properties, magnetic and physical parameters [9,10]. For this reason numerous papers and reviews are devoted to creation of MNCs that have required properties and are effective for specific applications [9–18]. The MNPs used in biomedicine are subject to strict requirements: biological compatibility, biodegradability, high colloidal stability. In addition, these MNPs shall be successfully delivered to a given organ, and in small quantities and, therefore, they shall be highly efficient, as, for example, when generating heat in MHT [7].

Numerous studies have shown that magnetic materials of spinel ferrites (SF) (MFe_2O_4, where M — metal ions), have the required parameters for MF. Studies have shown that ferrite $CoFe_2O_4$ has the most important properties for MF among the spinel ferrites, adaptable by the divalent metals

Mn, Mg, Ni, Zn, etc. introduced into the ferrite [11–18]. The wide range of applications of spinel ferrites MNP is determined by the fact that parameters such as particle size, particle size distribution, crystallite shape, ion distribution over non-equivalent lattice positions, etc. are very sensitive to factors such as synthesis method, chemical composition, annealing temperatures. All this allows controlling the properties of spinel ferrites during synthesis and obtaining spinel ferrites with the required characteristics [12–26].

For biomedical applications, as it has been found in recent years, the most attractive spinel is $CoFe_2O_4$, in which cobalt is replaced by ions of Zn ions ($Co_{1-x}Zn_xFe_2O_4$) [14,19–28]. The controlled synthesis of high-quality MNPs spinel ferrites and the study of their properties are attributable to both the need to understand the basics of nanomagnetism from a scientific point of view and to their adaptations for a variety of practical applications. $Co_{1-x}Zn_xFe_2O_4$ spinel ferrites are synthesized by various synthesis methods such as hydrothermal, combustion, ball mill grinding, sol-gel, wet chemical sintering, spark plasma sintering, co-precipitation and also a combination of these techniques with high-temperature calcination [3,9,10,13–17]. Various applications of such materials are shown in Ref. [18,19,23–30].

This paper is devoted to the synthesis by co-precipitation of MNPs $CoFe_2O_4$ with substitution of Co with Zn ions ($0.0 \leq x \leq 1.0$) and studies of structural, microstructural, and magnetic properties of ferrites $Co_{1-x}Zn_xFe_2O_4$ (hereinafter CZFO). The synthesized CZFO MNPs were studied by X-ray diffraction (XRD), Raman scattering spectroscopy, magnetic measurements and Mössbauer spectroscopy.

2. Materials and methods of experiments

2.1. Synthesis of MNP $Co_{1-x}Zn_xFe_2O_4$ (where $x = 0.0, 0.2, 0.4, 0.6, 0.8$ and 1.0)

There is no single global synthesis method that could be applied to create MNPs with desired chemical and physical characteristics. The method used for synthesis depends on the required set of particle properties. The method of co-precipitation has a number of advantages: low-cost and environment friendly reagents are used, instead of hazardous organic solvents; significantly short reaction time; high crystallinity of particles, no special washing procedures (see [30] and references there). The synthesis of MNPs of spinel ferrites of $Co_{1-x}Zn_xFe_2O_4$ ($x = 0.0$, 0.2, 0.4, 0.6, 0.8 and 1.0) based on the above was performed by the method chemical co-precipitation [31], modified by the authors [18]. The calculated amount of salts of $FeCl_3 \cdot 6H_2O$ (97%), $CoCl_2 \cdot 6H_2O$ (97%), $ZnCl_2$ (99%) was dissolved in distilled water (DW) separately with careful stirring for obtaining stoichiometric compositions. The obtained solutions were taken in appropriate quantities for the synthesis of the SF of the required compositions, and were intensively mixed for 1 h to improve the homogeneity of the solution mixture. A heated NaOH (2 M) solution was added to the resulting mixture in drops as a precipitating agent for achieving pH = 10 and for co-precipitation. The resulting mixture was kept at 80°C for 60 minutes and then cooled to room temperature. The synthesized powders were filtered, the resulting precipitate was washed in DW using magnetic decantation and then dried in an electric furnace at a temperature of 60° C for 12 h. The dried powder was crushed in an agate mortar and fired at a temperature of 300°C for 3 h for obtaining nanoscale particles. The synthesized materials were analyzed using SEM-EDS, and it was found that the compositions of the obtained powders were consistent with the components used for the synthesis of spinel ferrite particles of $Co_{1-x}Zn_xFe_2O_4$ (at $x = 0.0$, 0.2, 0.4, 0.6, 0.8, 1.0). X-ray powder diffractometer (XRD), vibration magnetometer (VM), infrared and Mössbauer spectroscopy were used for structural, morphological and magnetic studies of synthesized powders.

The phase composition of synthesized CZFO MNPs and crystallite sizes were determined from the X-ray diffraction profile using a Shimadzu-6100 X-ray powder diffractometer with Cu-$K\alpha$ radiation at a wavelength o$\lambda = 1.542$ A in the angle range 2θ, from 20 to 80° with scanning speed $1^\circ\,\mathrm{min}^{-1}$. The average size of the crystallites in the samples was calculated from the width of the diffraction line of maximum intensity (311) using the Scherrer formula [32].

Raman scattering spectra were obtained in the range ($200-900\,\mathrm{cm}^{-1}$) using Jobin-Yvon spectrometer (T64000) and a detector with a charge-coupled device with liquid nitrogen cooling. An argon-ion laser line with a wavelength of 514.5nm with a power of ~ 0, 2 mW was used for optical excitation of the samples. All spectra were obtained at room temperature.

The magnetic properties of the studied samples were studied using a vibrating magnetometer at a maximum value of the applied magnetic field of 10 kOe at room temperature. Saturation magnetizations (M_s), residual magnetizations (Mr) and coercivity (Hc) were determined from the obtained hysteresis loops.

Mössbauer spectroscopy was used to study the properties of synthesized MNPs, which is an informative method for studying materials. The Mössbauer measurements were performed on the isotope ^{57}Fe with recording of gamma radiation in the transmission geometry through the studied sample. The reference signal in the system of motion of the Doppler modulator in the spectrometer had a shape of triangle to set a speed with constant acceleration. Co^{57} in the rhodium matrix was the source of γ-radiation. The speed scale was calibrated using a foil of α-Fe with a thickness of 6 mkm at room temperature, and calibration was carried out using a laser interferometer for higher accuracy. The studied MNPs were placed in a special plastic container to prevent oxidation in air. The amount of the sample according to the content of Fe^{57} was adjusted so that the content of the isotope Fe^{57} was $\sim 10\,\mathrm{mg/cm}^2$.

The Mössbauer spectra (MS) of the studied MNF CZFO were acquired at a room temperature. The experimental MS mathematical processing was carried out using the program [33], which describes spectral lines with Lorentzian

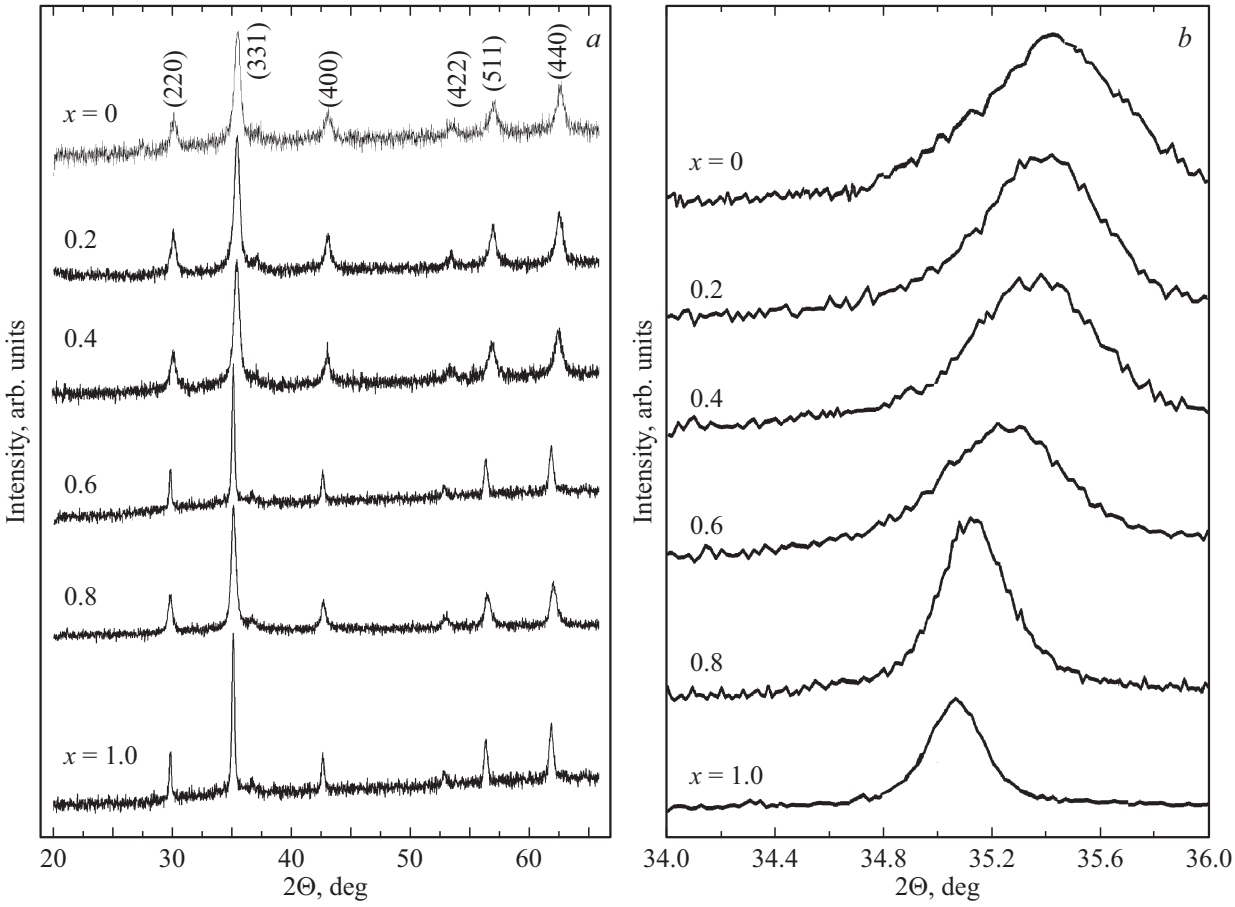

Figure 1. *a* — X-ray images of MNPs of $Co_{1-x}Zn_xFe_2O_4$ ($0 \le x \le 1.0$), *b* – the changed position of the peak of maximum intensity (311) depending on the zinc content.

peaks using the least-square method. The divergence of theoretical values of the hyperfine interaction (HFI) parameters is determined from the statistical deviations. The program searches for optimal values of parameters such as intensity, width and positions of spectral lines in the procedure of minimization of the functional of χ^2, The experimental MS processing was carried out taking into account contributions of ferrite-spinel corresponding to ions Fe^{3+} in octahedral and tetrahedral nodes of the spinel crystal lattice. The parameters of the hyperfine interactions (HFI) were calculated from the positions of the lines in MS: IS — the isomeric shift (mm/s), QS — the quadrupole shift (mm/s) and H_{eff} — the effective magnetic field (T) on iron ion nuclei. The divergence of theoretical values of the parameters of hyperfine interactions is determined from the statistical deviations [33].

3. Results and discussion thereof

3.1. Structural properties

Figure 1, *a* shows X-ray diffraction patterns (XRD) of synthesized CZFO MNPs. It should be noted that the diffraction patterns shown in Figure 1, *a* are similar to the lines published in [34–37]. Lines (220), (311), (400), (422), (511) and (440) observed in Figure 1, *a* agree well with the results shown on the maps of the International Diffraction Data Center (IJCD) for $CoFe_2O_4$ (IJCD№ 00-022-1086) and $Co_{1-x}Zn_xFe_2O_4$ (IJCD№ 98-016-6201 to −6204) and with Miller indices of the cubic spinel structure of the space group $Fd3m$. The large widths of the diffraction lines are explained by the nanometric sizes of the particles of the studied ferrites.

Figure 1, *b* shows that the diffraction peak shifts from a smaller angle to a larger one with the increase of concentration of Zn^{2+}. The shift of the peak position between the ferrites $CoFe_2O_4$ ($2\theta = 35.43°$) and $X_{1-x}Zn_xFe_2O_4$ ($2\theta = 35.06°$) is $\Delta\theta = 0.37°$, which is consistent with the values obtained in [34–37]. The lattice parameters and the average sizes of crystallites depending on the content of Zn ions are shown in Figure 2. The lattice constants were calculated using the distance between the two planes d and c with their corresponding parameters (hkl) and the obtained values confirm that the synthesized CZFO particles belong to cubic spinels. Figure 2 shows that the lattice constant increases from 8.375 to 8.430 Å with an increase in the number of ions of Zn^{2+} which is consistent with the literature data (for example [36]). The reason for the

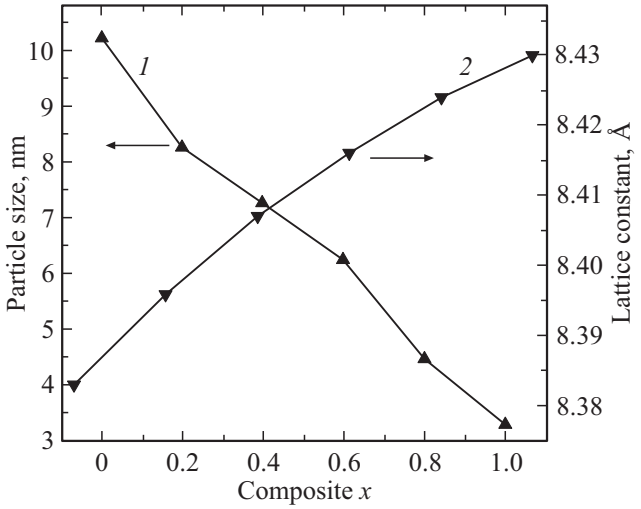

Figure 2. *1* — the crystallite sizes $Co_{1-x}Zn_xFe_2O_4$ ($0 \le x \le 1.0$) (1) and *2* — the lattice constants depending on the ion concentration Zn^{2+} (x) according to X-ray diffraction data.

increase of the lattice constant is that ions of Co^{2+} with a radius of 0.78 AA are replaced in ferrite $Co_{1-x}Zn_xFe_2O_4$ by larger ions of Zn^{2+} with a radius of (0.82 Å). The average crystallite sizes in the samples, calculated using the maximum intensity line width (311) according to the Scherrer formula [32] decrease from 10.5 to 3.4 nm with an increase of the content of ions of Zn^{2+} as can be seen in Figure 2.

3.2. Raman scattering spectroscopy of MNP of $Co_{1-x}Zn_xFe_2O_4$ ($0.0 \le x \le 1.0$)

Raman-scattering spectroscopy (Raman scattering — RS) is a non-destructive method that is very sensitive to the positions of cations that change the corresponding vibrational modes. Therefore, the RS is a method of identifying the structural properties of SF [36–43]. Oscillations of metal ions in the crystal lattice are usually observed in the range of 1000−400 cm^1.

Figure 3 shows the resonance Raman scattering (RS) spectra of CZFO MNPs at room temperature. It worth noting that the obtained spectra (Figure 3) are similar to the spectra published in Ref. [36–43]. All the features of RS of the light in the studied region can be attributed to the vibrational modes (A1g, Eg and 3T2g) of cubic spinel (space group $Fd3m$), which confirms the formation of spinel ferrite [36]. There are no signs of additional phases in the RS spectra (Figure 3). Figure 3 shows that the spectral bands are broadened, which is usually observed in case of inverse spinel ferrites. The broadening is attributable to the statistical distribution of Fe^{3+}, Zn^{2+} and Co^{2+} over (A) and [B] nonequivalent positions of the spinel crystal lattice. The changes of vibrational modes are observed depending on the number of Zn ions (Figure 3): *a* — ~ 620 and $\sim 670\,cm^{-1}$, *b* — $\sim 400\,cm^{-1}$ and *c* — $\sim 310\,cm^{-1}$. The integral intensity of the highest frequency mode of the RS ($\sim 620\,cm^{-1}$) decreases with the increase of Zn content (Figure 3). Figure 3 shows that the Raman mode at $\sim 670\,cm^{-1}$, is associated with oscillations of the bonds Fe-O4 or Co-O4, occupying (A) positions is not split, but includes modes of both bonds, which is similar to what is observed in Ref. [36]. The vibrational energy of the peak $\sim 670\,cm^{-1}$ does not change with an increase of the Zn content,which is consistent with the data of [36], but differs from the results obtained with an increase of the energy of such a peak with an increase of the number of Zn ions in the MNP of $Zn_xMg_{1-x}Fe_2O_4$ [43]. Thus, the number of bonds of Fe-O4 or Co-O4 in tetrahedral positions decreases with the increase of Zn content, which is consistent with the Mössbauer data.

The origin of vibrational modes in the region of 620−650 cm^{-1} remains controversial. For example, Ref. [43] attributed the mode $\sim 650\,cm^{-1}$ to the bonds of Zn-O6 in [B] positions. However, if this hypothesis is correct, then an increase of the integral area of this mode with an increase of the Zn content will indicate an increase of the number of bonds Zn-O6 in [B] nodes, which is inconsistent with the Mössbauer data indicating that the content of Zn^{2+} ions increases more sharply in (A) positions. Therefore, based on the trend observed in the Raman spectra, it can be argued that the mode at $\sim 650\,cm^{-1}$ belongs to the bonds of Zn-O4 in (A) positions, whereas the mode

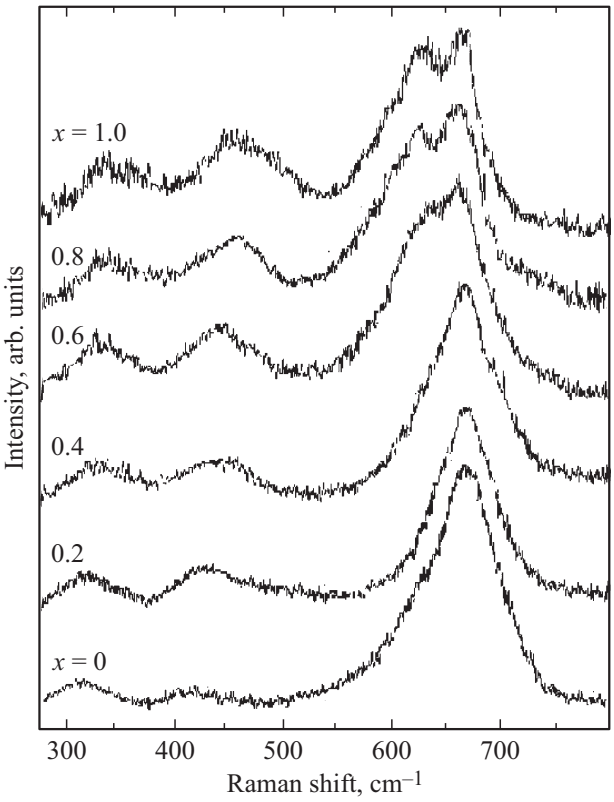

Figure 3. Raman spectra of MNP of $Co_{1-x}Zn_xFe_2O_4$ ($0 \le x \le 1.0$).

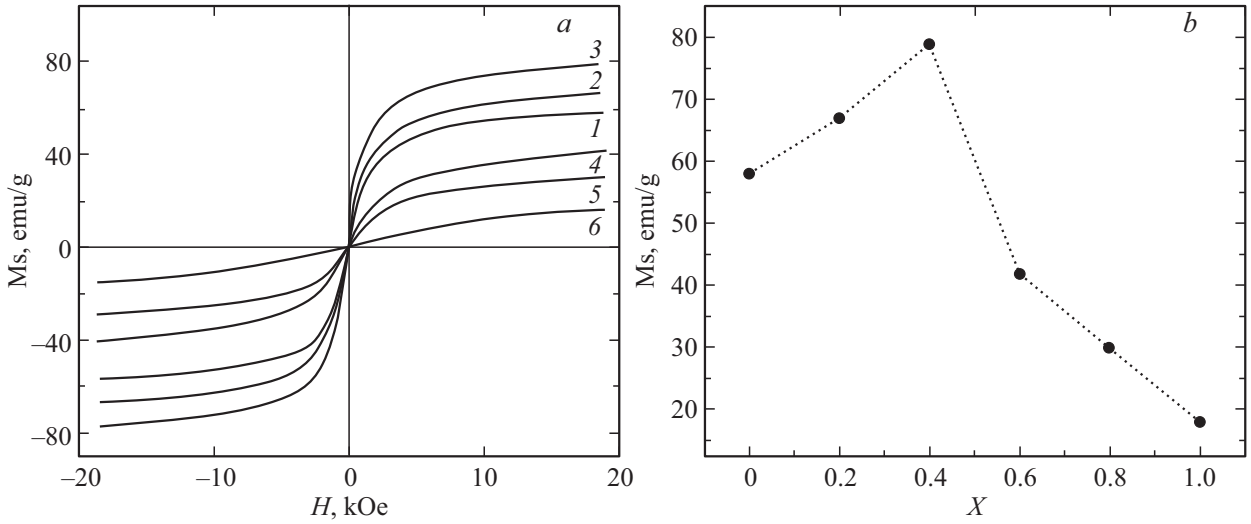

Figure 4. *a* — magnetic hysteresis loops of MNPs of $Co_{1-x}Zn_xFe_2O_4$ at room temperature in the field range from −20 to +20 kOe. Numbers *1, 2, 3, 4, 5* and *6* denote here the curves obtained with the ion substitution values of Zn^{2+} $x = 0.0$, 0.2, 0.4, 0.6, 0.8 and 1.0 respectively; *b* — the saturation magnetization (M_s) depending on the concentration (X) of Zn^{2+} ions in MNP of $Co_{1-x}Zn_xFe_2O_4$.

at 620 cm^{-1} should be attributed to Zn-O6 bonds in B-positions. However, the above picture does not agree with the observed features of Raman lines with a peak below 600 cm^{-1}. All these modes should have been associated with vibrations of M-O6 in octahedral positions according to the initial hypothesis. Therefore, any significant changes of Raman modes below 600 cm^{-1} cannot be expected with the preferential placement of ions of Zn^{2+} in (A) positions, since these modes would be associated with ion oscillations in [B] nodes.

3.3. Magnetic properties

Saturation magnetization (M_s) of CZFO MNPs at a room temperature are shown in Figure 4 depending on the concentration of Zn ($0 \le x \le 1.0$), measured in the region of external magnetic fields ±20 kOe. Figure 4, *a* shows that the value is $M_s = 67$ emu/g at $x = 0.2A$, and it becomes maximum (79 emu/g) at $x = 0.4$. The value decreases to 18 emu/g at $x = 1$ with a further increase of the Zn concentration. The value of M_s at $x = 0$, as seen in Figure4, *b* is ∼ 58 emu/g at 300 K, whereas it is equal to 81 emu/g for the volumetric analog [37,44]. The value of M_s in MNP of $Co_{1-x}Zn_xFe_2O_4$ synthesized by the sol-gel method [40] is similar to the value obtained in our study, and the value of M_s is slightly higher in the polyol synthesis of CZFO MNP (82 emu/g) [37]. Such an increase of M_s should be mainly attributable to a deviation of the structure from the thermodynamically stable distribution of cations, as assumed on the basis of structural studies [37]. It should be noted that the resulting value of $M_s = 79$ emu/g (Figure 4, *a*) is the largest for MNP of $Co_{1-x}Zn_xFe_2O_4$ synthesized by co-precipitation: 77.4 emu/g [24], 67 emu/g [30], 54 emu/g [45], and also more than the value of CZFO MNPs synthesized using other methods [14,35,41,46–50]. The spread of the values of the peaks M_s may be attributable to different distributions of cations over spinel sublattices, nonstoichiometry, and particle quality.

Spinel ferrites of cubic structure have nonequivalent tetrahedral (A) and octahedral [B] sublattices populated by metal ions and the magnetic ordering is determined by super-exchange interactions between the ions of these sublattices through oxygen ions. The magnetic moments of these sublattices in the Neel model are oriented antiparallel to each other [51] and their spin moments are collinear [52]. In this case, the total magnetization is equal to the difference of the total magnetic moments of M_B and M_A ions of the sublattices [B] and (A), respectively, i. e. $(M_B - M_A)$ [51]. The change of the magnetic moment (M_B) with an increase of the concentration of Zn^{2+} can be explained on the basis of the distribution of cations and the magnitude of super-exchange interactions of ions in (A) and [B] nodes. Ions of Zn^{2+} with zero magnetic moment and ions of Fe^{3+} have a strong preference for arrangement in a tetrahedral (A) sublattice. However, zinc ions introduced into the ferrite spinel displace Fe^{3+} ions from (A) to [B] nodes. Thus, the magnetization (A) of sublattice decreases because of the increase of the number of non-magnetic Zn ions in it, whereas the magnetic moment of [B] nodes increases because the number of ions of Fe^{3+} in [B] nodes increases as they are displaced by Zn ions from (A) to [B] positions. Thus, the total magnetization $(M_B - M_A)$ of the CZFO MNPs increases with an increase in the concentration of Zn $x = 0$ ions to $x = 0.4$ because of the changes in the super-exchange interactions of the magnetic ions of the sublattices (A) and [B]. The magnitudes of the magnetic moments M_A and M_B depending on the number of Zn ions were calculated in Ref.[24], using the distribution of metal ions (Fe^{3+}, Co^{2+} and Zn^{2+}) in MNP of $Co_{1-x}Zn_xFe_2O_4$.

Calculations showed that the value of M_B increases with the increase of zinc concentration to $x = 0.2$, which can be attributed to the collinear two-lattice model of Neel [51]. However, this model cannot explain the decrease of M_B (and therefore M_s) at concentrations of Zn greater than 0.2. It is necessary to the Japhet–Kittel model (J-K) [52] for this purpose, in which the crystal sublattice [B] of spinel is divided into two [B1] and [B2], whose magnetic moments are equal in magnitude, oppositely directed and canting, and the spin moments of the three ferrite sublattices form a triangular orientation. The maximum value of M_s should correspond to the transition from a collinear ferrimagnetic structure of the Neel type to a canting spin structure of the Japhet–Kittel type [53]. With an increase of the amount of Zn^{2+}, the dimensions of the CZFO MNP often decrease, which increases the surface/volume ratio and, some of the magnetic ions are missing due to the surface, reducing super-exchange interactions in the surface and subsurface layers. As a result, this leads to non-collinearity (canting structure) of the spin moments in the surface layer and a decrease in M_s.

3.4. Mössbauer studies of NP $Co_{1-x}Zn_xFe_2O_4$

Mössbauer spectroscopy provides unique data on the phase composition, local electronic configurations, magnetic structure and magnetic relaxation phenomena of nanoscale systems [18,30,54,55]. It should be noted that a large number of papers have been devoted to the Mössbauer studies of MNP of $Co_{1-x}Zn_xFe_2O_4$ [18,27–30,36,43,56–63]. Figure 5, *a* shows Mössbauer spectra (MS) of MNP of $Co_{1-x}Zn_xFe_2O_4$ SF at room temperature where the experimental values are shown by dots. Figure 5, *a* shows that the MS of CZFO MNP consist of Zeeman splitting lines that widen asymmetrically towards the center of the spectrum. Doublet lines appear against the background of ZS in the region of „of zero“ velocities at $x = 0.8$ on the MS, the intensity of which increases with an increase of the number of ions of Zn.

Experimental MS of MNP of $Co_{1-x}Zn_xFe_2O_4$ recorded at room temperature (Figure 5, *a*) are similar to those observed in [18,28–30,36,43,56–59] with appropriate numbers of Zn ions, but differ from those published in [61–63]. MS of MNP of $CoFe_2O_4$ shown in Figure 5, *a* differs from the spectra of macroscopic cobalt ferrite crystals, which show resolving lines of two ZS belonging to Fe ions in nonequivalent positions (A) and [B] of SF [64].

The mathematical processing of experimental MS of MNP of $Co_{1-x}Zn_xFe_2O_4$ cannot be performed only by two ZS belonging to Fe ions in nonequivalent lattice positions of a macroscopic spinel crystal due to the large width and asymmetry of the MS lines (Figure 5, *a*). Therefore, a model consisting of several ZS and, if necessary, a quadrupole doublet was used to process MS using the program [33]. The model ZS and doublets obtained during such processing are shown in Figure 5, *a* by lines with appropriate designations. The good consistency of the models used with the experimental MS of $Co_{1-x}Zn_xFe_2O_4$ MNP is indicated by the minimum values of the difference between the model and experimental values shown above each spectrum, as well as the values χ^2, located within 1.0−1.2. The HFI parameters listed in the table were calculated using the positions of spectral lines in MS of $Co_{1-x}Zn_xFe_2O_4$ MNP. Isomeric shifts (IS) are given relative to the metal foil α-Fe.

The impurity (secondary) phases of iron oxides appear on the MS of spinel ferrites as additional ZC or doublets, with HFI parameters. The lines of any impurity phase in quantities of at least 3 at.% iron can be easily identified on the MS. No secondary phase lines were found on the experimental MS of the CZFO MNP (Figure 5, *a*), which indicates the absence of additional phases in the studied MNP and this is consistent with the XRD and Raman scattering study data.

Fe^{2+} and Fe^{3+} ions are reliably identified in Mössbauer spectroscopy because of significant differences of their chemical shifts, varying from 0.2 to 0.5 mm/s for Fe^{3+}, and from 0.9 to 1.1 mm/s for Fe^{2+} [19]. It can be seen from the table that the IS values of Fe ions in the [B]- and (A)-positions are within 0.33−0.47 mm/s, which indicates the high-spin state of iron Fe^{3+}. This is consistent with the values of IS, which are in the range of 0.3−0.6 mm/s for SF. The values of chemical shifts from 0.9 to 1.1 mm/s belonging to iron ions in the low spin state of Fe^{2+} are missing.

One of the issues of Mössbauer spectroscopy is the determination of the affiliation of the observed ZS to Fe ions occupying the corresponding nonequivalent positions (A) and [B]. It is stated in [65] that the sextiplets with the largest values of IS and H_{eff} in MFe_2O_4 SF belong to ions of Fe^{3+} of octahedral [B] positions surrounded by the six nearest neighbors Fe^{3+}. A sextiplet with a lower IS value and H_{eff} refers to ions of Fe^{3+} tetrahedral (A) nodes [65]. Calculations in Ref. [66] showed that the covalence of the Fe(A)−O bond is greater than that of Fe[B]−O, which qualitatively explains why the spin density transfer from (A) to [B] ions in the spinel structure is more effective than the other way around. A number of studies showed that the hyperfine magnetic field of Fe ions in (A) nodes is greater than in the [B] nodes MFe_2O_4 SF [62,66–71]. Therefore, the relation of the ZS (Figure 2) to the iron ions of (A)- and [B]-sublattices was determined based on the value of H_{eff}, and not based on the values of IS, which coincide within the error limits for iron ions of (A) and [B] positions. The ZS with the largest value of H_{eff} is related to Fe ions in (A) nodes, sextiplets with successively decreasing fields in accordance with the contributions determined by the binomial distribution [66] refer to Fe ions occupying the [B] positions.

The MS presented in Figure 5, *a*, as well as in most papers on the Mössbauer studies of the SF consist of asymmetrically widened velocities of the ZS lines towards zero. Such spectra are formed by sextiplets belonging to iron ions in the spinel structure and surrounded by a different number of nearest Fe^{3+} neighbors. The number of nearest

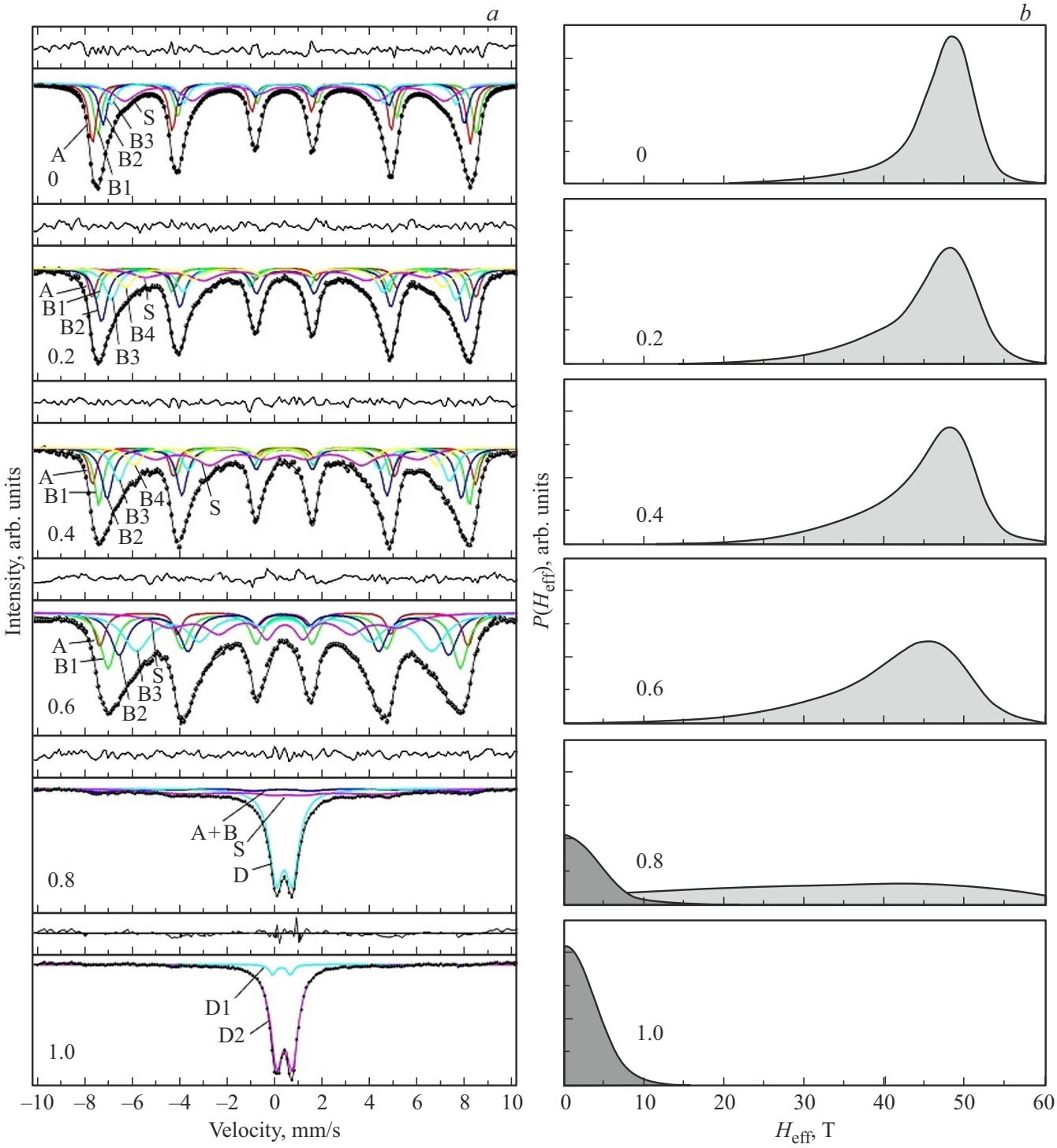

Figure 5. *a* — Mössbauer spectra of MNPs of $Co_{1-x}Zn_xFe_2O_4$ $(0 \le x \le 1.0)$ at room temperature. The dots show the experimental values, and the model components are shown by solid colored lines: The sextiplet (A) belongs to Fe ions in tetrahedral (A) positions, sextiplets B1, B2, B3 and B4 belpng to Fe ions in octahedral [B] nodes, paramagnetic doublet belong to D. Sextiplets S belong to Fe ions occupying positions in the surface layer of particles. *b* — the distribution functions $P(H_{eff})$ reconstructed from experimental Mössbauer spectra of MNP of $Co_{1-x}Zn_xFe_2O_4$ using the program [33].

neighbors is determined by the random placement of metal ions at the nodes of the crystal lattice and is described by the binomial distribution [66]:

$$P(k) = \binom{n}{k} p^k (1-p)^{n-k}, \ n = 6, \ k = 0, \ldots, 6, \quad (1)$$

where $P(k)$ is the probability of finding Zn atoms in the amount of k in the immediate environment of Fe atoms from the sublattice B, and p corresponds to the probability of finding Zn atoms in the sublattice A, in our case $p = x$.

The studied CZFO MNPs contain three different cations (iron, cobalt and zinc), which significantly increases the probability of a random distribution of these cations across the nodes of the crystal lattice and results in the formation of several octahedral [B] positions with different surrounding. The super-exchange interaction of (A)−[B] determines the hyperfine ion fields in (A) positions whose nearest neighbors are twelve ions in [B] positions and, therefore, less dependent on the random distribution of cations across [B] nodes. Only six cations of (A) nodes are the nearest neighbors for ions of Fe [B] positions. Consequently, a change of the distribution of cations at [B] positions by only 1/12 part affects the effective fields of Fe ions at (A) nodes, whereas the distribution of cations at (A) positions changes the effective ion field of Fe [B] nodes by 1/6 [66]. The transfer of spin density from (A) to [B] ions in the spinel structure is more efficient than the other way around, which can be qualitatively explained by the fact that the covalence of the Fe(A)−O bond is greater than the covalence of Fe[B]−O bond [66]. As a result, the effective magnetic field in the SF tested by (A) ions of Fe^{3+}, does not depend on the distribution of magnetic ions across [B] nodes, whereas the hyperfine [B] field of Fe ions significantly depends on the nearest ion surrounding of (A) nodes. Taking into account the above, the models used to process the MS of the CZFO MNPs gave a satisfactory conformance to the experimental MS according to the criterion χ^2.

MS of $CoFe_2O_4$ MNPs (Figure 5, *a*) when $x = 0$ consist only of sextiplets. An intense quadrupole doublet appears on the MS on the ZS background when the Zn quantity increases to $x = 0.8$. The sextiplets disappear when the number of Zn ions increases to $x = 1.0$, and only the paramagnetic doublet remains on the MS. Such changes in MS of $Co_{1-x}Zn_xFe_2O_4$ MNP with an increase of Zn concentration are explained by superparamagnetic relaxation [68,69]. The MS consists of a doublet If the relaxation time τ of nanoparticles is less than the time of the Mössbauer measurements ($\tau_M = 10^{-7}$ s for ^{57}Fe). A ZS with good line resolution is observed on the MS at $\tau \gg \tau_M$. The temperature at which the areas of the sextiplets and paramagnetic doublet are equal in the MS is called the blocking point T_b. The analysis of the spectral line areas of the components in the MS of $Co_{1-x}Zn_xFe_2O_4$ MNPs (table) suggests that the temperature T_b decreases with an increase of the number of Zn ions and it becomes lower than room temperature at $x = 0.8$, which is consistent with the data of magnetic measurements.

Figure 5, *a* shows that a sextiplet is observed on MS of $Co_{1-x}Zn_xFe_2O_4$ MNP, except for the sextiplets (A) and [B], which is denoted as S, whose effective fields are smaller than the fields of iron ions of (A) and [B] positions, and the line widths are much larger. Similar MS have been observed in many studies, for example, [36,43,56,69–71,72–79], but the reasons for the formation of such spectra have been explained in different ways (see [80] and the references there). It was assumed in [57,81,82], that the S-type sextiplet belongs to iron ions located in the surface layer of MNPs, but no arguments were given to support this assumption.

Let's consider the reasons for the formation of the S sextiplet in the MS of CZFO MNP. The theoretical foundations for the formation of ferrimagnetism in ferrites are given by Neel [51] on the basis of the super-exchange interaction of iron ions of tetra- (A) and octahedral [B] sublattices, orienting magnetic moments in antiparallel directions (antiferromagnetic ordering). The development of Neel's theory was the assumption of Japhet and Kittel (J-K) [52] that [B] sublattices are further subdivided so that the magnetic moments of all sublattices are arranged in the form of a triangle. The final confirmation of the Neel model for MNP was obtained by Mössbauer studies using large external magnetic fields (EMP) [79]. But, a special opinion was expressed in Ref. [83], based on the analysis of the line widths of the experimental MS of $NiFe_20_4$ MNP, that the particles should have a Japhet–Kittel spin structure. The existence of a canting structure J-K in MNP was confirmed by Mössbauer studies in large EMP [36,43,62,69–71,73–78], but it was not found that the canting structure belongs specifically to the surface layer of particles.

The assumption of the existence of a canting spin structure mainly on or near the surface was made on the basis of Mössbauer studies in large EMP of ultrafine particles γ-Fe_20_3 [84]. These particles were described as core/shell type MNPs, the core of which has an antiferromagnetic ordering of spin moments, and spin moments in the surface layer are oriented at some angle to their antiparallel direction in the core [84]. The Mössbauer spectroscopy in large EMP was widely used to confirm such a model (see [84,85] and references there). However, the heterogeneity of the ensemble of particles in size, superparamagnetic phenomena, strong dependence on the preparation technology, etc. significantly complicated the task of studying surface properties on the example of nanopowders. In addition, it is impossible to distinguish the magnetic structures of the volume and the surface layer of the particle using traditional Mössbauer spectroscopy data by transmittance of gamma radiation through a sample located in a large EMP. Nevertheless, explanations for the existence of a canting structure in the surface layer were justified by the exceptional role of the surface [86].

The existence of an anisotropic layer on the surface in ferromagnetic crystals was theoretically predicted by

Values of widths of the first and sixth lines (G) of Zeeman sextiplets, as well as isomeric shifts (IS), quadrupole splits (QS), effective magnetic fields (H_{eff}) and line areas (In) of Fe ions in tetrahedral (A), octahedral [B] positions, in the surface layer (S) and doublets (D) in $Co_{1-x}Zn_xFe_2O_4$ MNPs depending on the number of Zn ions (x)

X	Component	G (mm/s)	IS (mm/s)	QS (mm/s)	$H_{\text{eff}}(T)$	In (%)
0.0	A	0.374 ± 0.000	0.463 ± 0.004	0.002 ± 0.007	49.53 ± 0.03	20
	B1	0.382 ± 0.000	0.230 ± 0.003	0.014 ± 0.006	48.87 ± 0.03	26
	B2	0.417 ± 0.000	0.328 ± 0.005	0.022 ± 0.009	46.99 ± 0.06	17
	B3	0.491 ± 0.000	0.323 ± 0.006	0.004 ± 0.013	44.90 ± 0.08	13
	S	1.198 ± 0.077	0.367 ± 0.012	0.029 ± 0.022	41.64 ± 0.16	24
0.2	A	0.392 ± 0.000	0.371 ± 0.006	0.070 ± 0.011	49.95 ± 0.06	11
	B1	0.427 ± 0.000	0.253 ± 0.005	0.138 ± 0.009	48.82 ± 0.09	14
	B2	0.560 ± 0.000	0.354 ± 0.004	0.068 ± 0.008	47.42 ± 0.06	29
	B3	0.608 ± 0.000	0.311 ± 0.007	0.021 ± 0.014	44.86 ± 0.07	18
	B4	0.803 ± 0.000	0.375 ± 0.013	0.059 ± 0.027	41.35 ± 0.13	13
	S	1.462 ± 0.000	0.393 ± 0.029	0.045 ± 0.050	36.63 ± 0.32	15
0.4	A	0.392 ± 0.000	0.335 ± 0.006	0.005 ± 0.011	49.84 ± 0.07	12
	B1	0.441 ± 0.057	0.328 ± 0.005	0.012 ± 0.010	48.21 ± 0.07	17
	B2	0.555 ± 0.000	0.343 ± 0.004	0.010 ± 0.009	46.08 ± 0.10	25
	B3	0.663 ± 0.000	0.341 ± 0.009	0.001 ± 0.017	43.04 ± 0.11	17
	B4	0.668 ± 0.000	0.372 ± 0.015	0.036 ± 0.030	39.40 ± 0.17	10
	S	1.462 ± 0.000	0.413 ± 0.031	0.030 ± 0.052	34.21 ± 0.42	19
0.6	A	0.520 ± 0.024	0.331 ± 0.004	0.005 ± 0.008	47.90 ± 0.05	10
	B1	0.745 ± 0.000	0.342 ± 0.003	0.001 ± 0.007	45.82 ± 0.07	24
	B2	0.857 ± 0.000	0.317 ± 0.004	0.022 ± 0.007	42.87 ± 0.06	21
	B3	1.340 ± 0.000	0.353 ± 0.006	0.037 ± 0.010	38.41 ± 0.08	26
	S	1.734 ± 0.000	0.347 ± 0.013	0.040 ± 0.024	29.69 ± 0.16	19
0.8	A + B	1.689 ± 0.000	0.268 ± 0.040	0.053 ± 0.078	47.18 ± 0.24	12
	S	3.380 ± 0.000	0.401 ± 0.048	0.196 ± 0.084	25.47 ± 0.48	28
	D	0.669 ± 0.009	0.339 ± 0.001	0.679 ± 0.004	–	60
1.0	D1	0.313 ± 0.059	0.223 ± 0.014	0.735 ± 0.017	–	6
	D2	0.607 ± 0.006	0.350 ± 0.005	0.655 ± 0.003	–	94

L. Neel in 1954 [87]. However, experimental studies of the structure and properties of the surface layer attracted attention much later (see [88–90] and references there), and property studies were conducted on thin films and nanoscale powders, because the surface/volume ratio increases many times in these materials and the surface spins of Fe ions become dominant. But, as mentioned above, such materials are challenging for studying the properties of the surface and volume.

All these difficulties are overcome in case of usage of macroscopic crystals, but there were no techniques in those years that allow direct comparison of the properties of the surface layer of macrocrystals with bulk properties. New unique opportunities for studying properties and phase transitions in thin surface layers of macroscopic crystals using the method of „simultaneous gamma, X-ray and electron Mössbauer spectroscopy (SGXEMS)“, first proposed and implemented in an automated system [90–92]. The uniqueness of the SGXEMS method lies in the fact that the information provided on the properties of the surface layer and the volume of the crystal is extracted simultaneously, and using a single method (the Mössbauer effect), which allows direct comparison of experimentally obtained data on the state of the surface and volume of the crystal. Later, the SGXEMS method in foreign literature was called „Simultaneous Triple Radiation Mössbauer Spectroscopy (STRMS)“ [93,94].

The first direct experimental confirmation of the existence of a „transitional“ (in the terminology of that time) layer on the surface of macroscopic crystals of Fe_3BO_6, within which the orientation of the magnetic moments of iron ions smoothly deviates (as it approaches the surface) from directions in volume was obtained by the SGXEMS method [88,89]. The presence of a „transitional“ surface layer (or in modern terminology „of a canting structure“) in hexagonal ferrites $BaFe_{12}O_{19}$ and $SrFe_{12}O_{19}$, doped with diamagnetic ions Sc and Al, was first confirmed by SGXEMS method [95–98]. The transitional surface layer was not found in $MFe_{12}O_{19}$ hexaferrites (where M — Ba, Sr or Pb) without diamagnetic substitution by the SGXEMS method [99]. The analysis of model MS for $MFe_{12}O_{19}$ ferrites showed that the thickness of the transitional layer in these crystals cannot exceed units of nm [99], which is less than the experimental accuracy

of ~ 5 nm, but coincides with the value obtained from theoretical calculations by Neel [87]. Consequently, the doping of hexaferrite crystals with diamagnetic ions resulted in the breakage of super-exchange bonds that complement the breaks due to the surface, and the thickness of the „transitional" layer (or a layer with a „canting structure") increases [95–98]. The transitional surface layer (or a canting spin structure) [95–98] found on the surface of ferrite macrocrystals should be preserved even when the crystallite sizes are reduced to nanowalls.

It can be stated that the sextiplet S belongs to Fe ions in the CZFO MNP whose nearest neighbors are one or two magnetic ions. However, the table shows that the difference of the values of H_{eff} ions of [B] sublattice and sextiplet S is significantly greater than in case of substitution of one or even two Fe ions with diamagnetic one [66] in the immediate environment of [B] ions. The large line widths of the S component and the large difference of the effective fields of the S and [B] sextiplets indicate that the S sextiplet is formed by surface and subsurface iron ions that lost some of the super-exchange bonds, both due to the surface and diamagnetic ions.

It should be noted that the state with different magnetic structures of the volume and the surface layer in the SF MNP cannot be observed by other methods other than Mössbauer spectroscopy. This is explained by the fact that SF MNP are single-phase, well crystallized, and consist of a single material. This distinguishes SF particles from core/shell composites, in which the core and shell are made of different magnets, for example, magnetite and maghemite [100]. Therefore, the results of the work were confirmed by the Mössbauer studies [30,80], in which, for the first time without the use of high magnetic fields (expensive equipment), it was shown that the volume and surface layer of SF particles have different magnetic structures: the particles are ordered ferromagnetically in the volume (non-Gel structure), and they are ordered ferrimagnetically in the surface layer (Japhet–Kittel structure).

3.5. Distribution of effective magnetic fields $P(H_{\text{eff}})$ in $Co_{1-x}Zn_xFe_2O_4$

The use of Lorentzian lines in the absence of resolution of sextiplets is not effective to obtain the distribution functions of the effective magnetic field $P(H_{\text{eff}})$, which occurs due to the local inhomogeneity of the cation distribution. The most reliable method is the MS processing using the Voigt function as a spectral line if Fe ions are located in different types of local environment [101,102]. Therefore, functions $P(H_{\text{eff}})$ were restored using the program [33] describing MS by Voigt lines from the experimental MS of $Co_{1-x}Zn_xFe_2O_4$ MNPs (Figure 5, *b*). Function $P(H_{\text{eff}})$ at $x = 0$ (Figure 5, *b*) differ from the curve $P(H_{\text{eff}})$ of the macrocrystals of $CoFe_2O_4$ SF, at which two maxima of iron ions are observed, occupying nonequivalent positions (A) and [B] in the ferrite structure [64].

A peak is observed at $x \leq 0.4$ on the functions obtained for MNP of $Co_{1-x}Zn_xFe_2O_4$ (Figure 5, *b*) $P(H_{\text{eff}})$, that is asymmetric in the direction of smaller effective field values. This asymmetry is explained by the fact that Fe ions in the [B] sublattice have a different number of Fe ions in their environment, described by the distribution (1). The position of the peak shifts towards smaller ones effective fields with an increase of the number of substitution ions Zn (Figure 5, *b*) indicating that the substitution of Zn ions results in a decrease of H_{eff} and the proportion of the magnetically ordered state. At the same time, the intensity of the line in the range from 0 to 1.3 T, corresponding to the doublet lines in MS, increases. Zeeman lines and a paramagnetic phase line are observed on the function $P(H_{\text{eff}})$ at $x = 0.6$ suggesting that some fraction of the MNP underwent transition into the paramagnetic state. All particles are in the paramagnetic phase at $x = 1.0$. The features of the functions $P(H_{\text{eff}})$ (Figure 5, *b*) reflect the complex magnetic structure of the studied MNPs of $Co_{1-x}Zn_xFe_2O_4$, which cannot be explained only by the redistribution of Zn ions surrounding iron ions, and it is necessary to take into account the impact of the surface.

The analysis of experimental Mössbauer spectra (Figure 5, *a*) and published results of Mössbauer studies (see [30] and references there) suggests that the sizes of the studied CZFO MNPs vary from 15 up to 4 nm, when Zn ions are substituted from 0.0 to 1.0, which is consistent with the X-ray data.

4. Conclusion

The systematic studies of $Co_{1-x}Zn_xFe_2O_4$ MNPs were carried out, depending on the concentration of Zn ions ($x = 0.0$, 0.2, 0.4, 0.6, 0.8 and 1.0), synthesized by a simple co-precipitation method. The structural and morphological properties of MNPs were studied using X-ray diffraction (XRD), Raman and Mössbauer spectroscopy. Data from XRD, Raman scattering and Mössbauer spectroscopy confirm that the studied particles are single-phase and have a cubic structure of spinel ferrites (FS) $Co_{1-x}Zn_xFe_2O_4$ (space group $Fd3m$) in the entire range of substitution by Zn ions. It was found by the Raman scattering method, that $CoFe_2O_4$ MNPs have a normal spinel structure, and Co^{2+} and Fe^{3+} cations are redistributed between tetra- and octahedral positions when doped with Zn^{2+} ions and the structure is transformed into a mixed ferrite. It was found that the average crystallite sizes decrease from 10 to 3 nm and from 15 to 4 nm, respectively with an increase of the number of Zn ions from $x = 0.0$ to $x = 1.0$ based on X-ray diffraction and Mössbauer data. Experimental Mössbauer spectra indicate the typical superparamagnetic behavior of $Co_{1-x}Zn_xFe_2O_4$ MNPs. The introduction of Zn ions into $Co_{1-x}Zn_xFe_2O_4$ at $x > 0.6$ results in the transition to the paramagnetic state of a thin layer on the surface of particles, the thickness of which increases with the increase

of the number of introduced Zn ions, and the entire particle becomes paramagnetic at $x = 1.0$.

The conclusions of the papers [30,80] were confirmed, which showed for the first time using Mössbauer spectroscopy without an external magnetic field that there is a canting spin structure of the Jafert–Kittel type on the surface of ferrite MNPs, due to the impact of the surface, whereas there is a collinear ordering of spin moments of the Nelev type in the volume of particles. The mechanism of the evolution of SF MNPs from a magnetically ordered state to a paramagnetic state with the introduction of paramagnetic ions is described. The results obtained are important for the development and creation of magnetic nanoparticles for various applications, including biomedical ones.

Conflict of interest

The authors declare that they have no conflict of interest.

References

[1] J.A. Ramos-Guivar, E.O. Lopez, J.-M. Greneche, F.J. Litterst, E.C. Passamani. Appl. Surf. Sci. **538**, 148021 (2021). https://doi.org/10.1016/j.apsusc.2020.148021

[2] M. Abdolrahimi, M. Vasilakaki, S. Slimani, N. Ntallis, G. Varvaro, S. Laureti, C. Meneghini, K.N. Trohidou, D. Fiorani, D. Peddis. Nanomater. **11**, *7*, 1787 (2021). https://doi.org/10.3390/nano11071787

[3] S.A. Novopashin, M.A. Serebryakova, S.Ya. Khmel. Teplofizika i aeromekhanika **22**, *4*, 411 (2015). (in Russian).

[4] V.A. Suchilin, I.E. Gribut, S.A. Golikov. Elektrotekh. i inform. komplekses and sistemy **7**, *4*, 41 (2011). (in Russian).

[5] E.M. Materon, C.M. Miyazaki, O. Carr, N. Joshi, P.H.S. Picciani, C.J. Dalmaschio, F. Davis, F.M. Shimizu. Appl. Surf. Sci. Adv. **6**, 100163 (2021). https://doi.org/10.1016/j.apsadv.2021.100163

[6] M.G.M. Schneider, M.J. Martín, J. Otarola, E. Vakarelska, V. Simeonov, V. Lassalle, M. Nedyalkova. Pharmaceutics **14**, *1*, 204 (2022). https://doi.org/10.3390/pharmaceutics14010204

[7] I.M. Obaidat, V. Narayanaswamy, S. Alaabed, S. Sambasivam, C.V.V.M. Gopi. Magnetochemistry **5**, *4*, 67 (2019). DOI: 10.3390/magnetochemistry5040067

[8] A. Purohit, L. Soni, L. Thakur, J. Shrivastava, K. Khan, K. Shrivastava, S. Jain. Internat. J. Med. Sci. Pharma Res. **8**, *4*, 1 (2022). DOI: http://dx.doi.org/10.22270/ijmspr.v8i4.50.

[9] Magnetic Nanoferrites and their Composites / Eds Susheel Kalia, Rohit Jasrotia, Virender Pratap Singh. Elsevier Ltd. (2023). https://doi.org/10.1016/B978-0-323-96115-8.00004-0.

[10] Springer Ser. Mater. Sci. / Eds D. Peddis, S. Laureti, D. Fiorani. New Trends in Nanoparticle Magnetism. Part IV. Advanced Magnetic Nanoparticles Systems for Applications. V. 308. 2021. P. 301. https://doi.org/10.1007/978-3-030-60473-8.

[11] V. Socoliuc, D. Peddis, V.I. Petrenko, M.V. Avdeev, D. Susan-Resiga, T. Szabó, R. Turcu, E. Tombácz, L. Vékás. Magnetochem. **6**, 2 (2020). DOI: 10.3390/magnetochemistry6010002.

[12] B. Wareppam, E. Kuzmann, V.K. Garg, L.H. Singh. J. Mater. Res. **38**, 937 (2023). DOI:10.1557/s43578-022-00665-4.

[13] Ferrite Nanostructured Magnetic Materials / Eds J.P. Singh, K.H. Chae, R.C. Srivastava, O.F. Caltun. Woodhead Publishing Series Elsevier Ltd. (2023). 892 p. https://doi.org/10.1016/C2020-0-00253-7.

[14] P.A. Vinosha, A. Manikandan, A.S.J. Ceicilia, A. Dinesh, G.F. Nirmala, A.C. Preetha, Y. Slimani, M.A. Almessiere, A. Baykal, B. Xavier. Ceram. Int. **47**, 10512 (2021). https://doi.org/10.1016/j.ceramint.2020.12.289

[15] Syed Ismail Ahmad. J. Magn. Magn. Mater. **562**, 169840 (2022). https://doi.org/10.1016/j.jmmm.2022.169840

[16] M. Sajid, J. Płotka-Wasylka. Microchem. J. **154**, 104623 (2020). https://doi.org/10.1016/j.microc.2020.104623.

[17] F. Sharifianjazi, M. Moradi, N. Parvin, A. Nemati, A.J. Rad, N. Sheysi, A. Abouchenari, A. Mohammadi, S. Karbasi, Z. Ahmadi, A. Esmaeilkhanian, M. Irani, A. Pakseresht, S. Sahmani, M.S. Asl. Ceram. Int. **46**, 18391 (2020). https://doi.org/10.1016/j.ceramint.2020.04.202.

[18] A.S. Kamzin, D.S. Nikam, S.H. Pawar. Phys. Solid State **59**, *1*, 156 (2022). DOI: 10.1134/S1063783417010127

[19] A.S. Kamzin, I.M. Obaidat, V.G. Semenov, V. Narayanaswamy, I.A. Al-Omari, B. Issa, I.V. Buryanenko. Phys. Solid State **64**, *6*, 714 (2022). DOI: 10.21883/PSS.2022.06.53838.298.

[20] K.K. Kefeni, T.A.M. Msagati, T.T.I. Nkambule, B.B. Mamba. Mater. Sci. Eng. C **107**, 110314 (2020). https://doi.org/10.1016/j.msec.2019.110314

[21] A. Mittal, I. Roy, S. Gandhi. Magnetochem, **8**, 107 (2022). https://doi.org/10.3390/magnetochemistry8090107

[22] C. Janko, T. Ratschker, K. Nguyen, L. Zschiesche, R. Tietze, S. Lyer, C. Alexiou. Frontiers Oncology **9**, 59 (2019). DOI: 10.3389/fonc.2019.00059

[23] O.F. Odio, E. Reguera. In: Magnetic Spinels — Synthesis, Properties and Applications. IntechOpen. (2017). Ch. 9. P. 186. http://dx.doi.org/10.5772/67513/.

[24] D.S. Nikam, S.V. Jadhav, V.M. Khot, R.A. Bohara, C.K. Hong, S.S. Mali, S.H. Pawar. RSC Adv. **5**, 2338 (2015). DOI: 10.1039/c4ra08342c

[25] J. Mohapatra, M. Xing, J.P. Liu. Materials **12**, 3208 (2019). DOI: 10.3390/ma12193208.

[26] M. Albino, E. Fantechi, C. Innocenti, A. López-Ortega, V. Bonanni, G. Campo, F. Pineider, M. Gurioli, P. Arosio, T. Orlando et al. J. Phys. Chem. C **123**, 6148 (2019).

[27] V. Mameli, A. Musinu, A. Ardu, G. Ennas, D. Peddis, D. Niznansky, C. Sangregorio, C. Innocenti, N.T.K. Thanh, C. Cannas. Nanoscale **8**, 10124 (2016).

[28] M.M. Naik, H.S.B. Naik, G. Nagaraju, M. Vinuth, K. Vinu, R. Viswanath. Nano-Struct. Nano-Objects **19**, 100322 (2019). https://doi.org/10.1016/j.nanoso.2019.100322

[29] V. Pilati, R.C. Gomes, G. Gomide, P. Coppola, F.G. Silva, F.L.O. Paula, R. Perzynski, G.F. Goya, R. Aquino, J. Depeyrot. J. Phys. Chem. C **122**, 3028 (2018).

[30] A.S. Kamzin, I.M. Obaidat, V.G. Semenov, V. Narayanaswamy, I.A. Al-Omari, B. Issa, I.V. Buryanenko. Phys. Solid State **65**, *3*, 470 (2023). DOI: 10.21883/PSS.2023.03.55591.544

[31] T. Iwamoto, T. Ishigaki. J. Phys.: Conf. Ser. **441**, 012 034 (2013).

[32] P. Scherrer. Göttinger Nachrichten Math. Phys. **2**, 98 (1918).

[33] V.G. Semenov, V.V. Panchuk. Mössbauer Spectra Processing Software MossFit. Private message.

[34] M. Sundararajana, V. Sailajab, L.J. Kennedya, J.J. Vijaya. Ceram. Int. **43**, 540 (2017). http://dx.doi.org/10.1016/j.ceramint.2016.09.191
[35] A. Omelyanchik, K. Levada, S. Pshenichnikov, M. Abdolrahim, M. Baricic, A. Kapitunova, A. Galieva, S. Sukhikh, L. Astakhova, S. Antipov, B. Fabiano, D. Peddis, V. Rodionova. Materials **13**, 5014 (2020). DOI: 10.3390/ma13215014
[36] F. Nakagomi, P.E.N. de Souza, T.J. Castro, V.K. Garg, A.C. Oliveira, F.C. de Silva, Franco Jr., P.C. Morais, S.W. da Silva. J. All. Comp. **842**, 155751 (2020). https://doi.org/10.1016/j.jallcom.2020.155751
[37] L.B. Tahar, H. Basti, F. Herbst, L.S. Smiri, J.P. Quisefit, N. Yaacoub, J.M. Grenèche, S. Ammar. Mater. Res. Bull. **47**, 2590 (2012). http://dx.doi.org/10.1016/j.materresbull.2012.04.080
[38] P. Monisha, P. Priyadharshini, S.S. Gomathi, M. Mahendran, K. Pushpanathan. App. Phys. A **125**, 736 (2019). https://doi.org/10.1007/s00339-019-3014-x.
[39] V.K. Lakshmi, G.S. Kumar, A. Anugraha, T. Raguram, K.S. Rajni. IOP Conf. Ser.: Mater. Sci. Eng. **577**, 012068 (2019). DOI: 10.1088/1757-899X/577/1/012068.
[40] J.P. Singh, R.C. Srivastava, H.M. Agrawal, R. Kumar. J. Raman Spectrosc. **42**, 1510 (2011). DOI: 10.1002/jrs.2902.
[41] P.T. Phong, P.H. Nam, N.X. Phuc, B.T. Huy, L.T. Lu, D.H. Manh, IN-JA Lee. Met. Mater. Trans. A **50**, 1571 (2019). https://doi.org/10.1007/s11661-018-5096-z
[42] R.S. Yadav, J. Havlica, M. Hnatko, P. Šajgalík, C. Alexander, M. Palou, E. Bartoníčková, M. Boháč, F. Frajkorová, J. Masilko, M. Zmrzlý, L. Kalina, M. Hajdúchová, V. Enev. J. Magn. Magn. Mater. **378**, 190 (2015). https://doi.org/10.1016/j.jmmm.2014.11.027.
[43] S.W. da Silva, M. Naik, F. Nakagomi, M.S. Silva, A. Franco Jr., V.K. Garg, A.C. Oliveira, P.C. Morais. J. Nanopart. Res. **14**, 798 (2012). DOI: 10.1007/s11051-012-0798-4.
[44] J. Smit, H.P.J. Wijn. Les ferrites. Les Proprietes: Physiques des Oxydes Ferrimagnetiques en Relation avec leurs Applications Techniques. Bibliothe‘que Technique de Philips. (1961). P. 400.
[45] R. Arulmurugana, G. Vaidyanathana, S. Sendhilnathanb, B. Jeyadevan. Physica B **363**, 225 (2005). DOI: 10.1016/j.physb.2005.03.025
[46] G. Vaidyanathana, S. Sendhilnathan. Phys. B **403**, 2157 (2008). DOI: 10.1016/j.physb.2007.08.219.
[47] Y.S. Gaiduk, E.V. Korobko, K.A. Shevtsova, D.A. Kotikov, I.A. Svito, A.E. Usenko, D.V. Ivashenko, A. Fahmy, V.V. Pankov. Kondensirovannye sredy i mezhfaznye granitsy, **22**, *1*, 28 (2020). (in Russian). DOI: https://doi.org/10.17308/kcmf.2020.22/2526
[48] H.L. Andersen, C. Granados-Miralles, M. Saura-Múzquiz, M. Stingaciu, J. Larsen, F. Søndergaard-Pedersen, J.V. Ahlburg, L. Keller, C. Frandsen, M. Christensen. Mater. Chem. Front. **3**, 668 (2019). DOI: 10.1039/c9qm00012g.
[49] H. Malik, A. Mahmood, K. Mahmood, M.Y. Lodhi, M.F. Warsib, I. Shakirc, H. Wahab, M. Asghar, M.A. Khan. Ceram. Int. **40**, 9439 (2014). http://dx.doi.org/10.1016/j.ceramint.2014.02.015.
[50] X.H. Li, C.L. Xu, X.H. Han, L. Qiao, T. Wang, F.S. Li. Nanoscale Res. Lett. **5**, 1039 (2010).
[51] L. Neel. Ann. Phys. (Paris) **3**, 137 (1948).
[52] Y. Yafet, C. Kittel. Phys. Rev. **87**, *2*, 290 (1952). DOI: 10.1103/physrev.87.290 10.1103/PhysRev.87.290
[53] S. Chikazumi. Physics of ferromagnetism. Oxford University Press, Oxford (1997). P. 502.
[54] Applications of Mössbauer Spectroscopy. 1st ed. / Ed. R.L. Cohen. Elsevier (1980).
[55] V. Kuncser, O. Crisan, G. Schinteie, F. Tolea, P. Palade, M. Valeanu, G. Filoti. Modern Trends in Nanoscience. Editura Academiei Romane, Bucharest (2013). V. 197.
[56] M.I.A.A. Maksoud, A. El-Ghandour, G.S. El-Sayyad, R.A. Fahim, A.H. El-Hanbaly, M. Bekhit, E.K. Abdel-Khalek, H.H. El-Bahnasawy, M.A. Elkodous, A.H. Ashour, A.S. Awed. J Inorg. Organomet. Polym. Mater. **30**, 3709 (2020). https://doi.org/10.1007/s10904-020-01523-8.
[57] V. Sepelak, D. Baabe, F.J. Litterst, K.D. Becker. J. App. Phys. **88**, *10*, 5884 (2000). DOI: 10.1063/1.1316048
[58] G.A. Petitt, D.W. Forester. Phys. Rev. B **4**, *11*, 3912 (1971).
[59] A. Ghasemi, V. Šepelák, S.E. Shirsath, X. Liu, A. Morisako. J. Appl. Phys. **109**, 07A512 (2011). DOI: 10.1063/1.3553777.
[60] W. Bayoumi. J. Mater. Sci. **42**, 8254 (2007). DOI: 10.1007/s10853-007-1616-8.
[61] Q. Lin, J. Xu, F. Yang, J. Lin, H. Yang, Y. He. Mater. **11**, 1799 (2018). DOI: 10.3390/ma11101799.
[62] T. Tatarchuk, N. Paliychuk, M. Pacia, W. Kaspera, W. Macyk, A. Kotarba, B.F. Bogacz, A.T. Pedziwiatr, I. Mironyuk, R. Gargula, P. Kurzydło, A. Shyichuk. New J. Chem. **43**, *7*, 3038 (2019). https://doi.org/10.1039/C8NJ05329D
[63] H.H. Joshi, P.B. Pandya, R.G. Kulkarni. Solid State Commun. **86**, *12*, 807 (1993).
[64] A. Bouhas, M. Amzal, B. Zouranen. Mater. Chem. Phys. **33**, *1–2*, 80 (1993). https://doi.org/10.1016/0254-0584(93)90094-3
[65] C.N. Chinnasamy, A. Narayanasamy, N. Ponpandian, K. Chattopadhyay, K. Shinoda, B. Jeyadevan, K. Tohji, K. Nakatsuka, T. Furubayashi, I. Nakatani. Phys. Rev. B **63**, *18*, 184108 (2001).
[66] G.A. Sawatzky, F. Van Der Woude, A.H. Morrish. Phys. Rev. **187**, *1*, 747 (1969).
[67] S.P. Yadav, S.S. Shinde, P. Bhatt, S.S. Meena, K.Y. Rajpure. J. Alloys Compd. **646**, 550 (2015). http://dx.doi.org/10.1016/j.jallcom.2015.05.270
[68] E. Lima Jr., E. De Biasi, M.V. Mansilla, M.E. Saleta, F. Effenberg, L.M. Rossi, R. Cohen, H.R. Rechenberg, R.D. Zysler. J. App. Phys. **108**, 103919 (2010). DOI: 10.1063/1.3514585
[69] S.C. Bhargava, P.K. Iyengar. Phys. Status Solidi B **53**, *1*, 359 (1972). https://doi.org/10.1002/pssb.2220530138
[70] A. Ramakrishna, N. Murali, T.W. Mammo, K. Samatha, V. Veeraiah. Phys. B: Condens. Matter. **534**, 134 (2018). https://doi.org/10.1016/j.physb.2018.01.033
[71] T.R. Tatarchuk, M. Bououdina, N.D. Paliychuk, I.P. Yaremiy, V.V. Moklyak. J. Alloy. Compd. **694**, 777 (2017). https://doi.org/10.1016/j.jallcom.2016.10.067
[72] M.M. Kothawale, R. Pednekar, U.B. Gawas, S.S. Meena, N. Prasad, S. Kumar. J. Supercond. Nov. Magn. **30**, *2*, 395 (2017).
[73] M. Hashim, S.S. Meena, R.K. Kotnala, S.E. Shirsath, P. Bhatt, S. Kumar, E. Sentürk, R. Kumar, N. Gupta, Alimuddin. J. Magn. Magn. Mater. **360**, 21 (2014). http://dx.doi.org/10.1016/j.jmmm.2014.01.047

[74] N. Velinov, E. Manova, T. Tsoncheva, C. Estournés, D. Paneva, K. Tenchev, V. Petkova, K. Koleva, B. Kunev, I. Mitov. Solid State Sci. **14**, 1092 (2012). Doi.10.1016/j.solidstatesciences.2012.05.023.
[75] R.S. de Biasi, L.H.G. Cardoso. Physica B **407**, *18*, 3893 (2012). http://dx.doi.org/10.1016/j.physb.2012.06.017
[76] J.Z. Msomi, W.B. Dlamini, T. Moyo, P. Ezekiel. J. Magn. Magn. Mater. **373**, 68 (2015). DOI: 10.1016/j.jmmm.2014.01.044
[77] B.F. Bogacz, R. Gargula, P. Kurzydło, A.T. Pedziwiatr, T. Tatarchuk, N. Paliychuk. Acta Phys. Polonica A **134**, *5*, 993 (2018).
[78] E. Wu, S.J. Campbell, W.A. Kaczmareka, M. Hofmann, S.J. Kennedy. Int. J. Mater. Res. **94**, *10*, 1127 (2003).
[79] J. Chappert, R.B. Frankel. Phys. Rev. Lett. **12**, 570 (1967).
[80] A.S. Kamzin, V.G. Semenov, I.A. Al-Omari, V. Narayanaswamy, B. Issa. Phys. Solid State **65**, *8*, 1363 (2022). DOI: 10.61011/PSS.2023.08.56586.122
[81] I.S. Lyubutin, S.S. Starchikov, T.V. Bukreeva, I.A. Lysenko, S.N. Sulyanov, N.Y. Korotkov, S.S. Rumyantseva, I.V. Marchenko, K.O. Funtov, A.L. Vasiliev. Mater. Sci. Eng. C **45**, 225 (2014). https://doi.org/10.1016/j.msec.2014.09.017
[82] I.S. Lyubutin, S.S. Starchikov, L. Chun-Rong, N.E. Gervits, N.Y. Korotkov, T.V. Bukreeva. Croat. Chem. Acta **88**, 397 (2015). https://doi.org/10.5562/cca2739
[83] D. Kedem, T. Rothem. Phys. Rev. Lett. **18**, 165 (1967).
[84] J.M.D. Coey. Phys. Rev. Lett. **27**, *17*, 1140 (1971).
[85] Mössbauer Spectroscopy Applied to Magnetism and Material Science / Eds G.J. Long, F. Grandjean. Plenum Press, N.Y. (1993). 479 p.
[86] I.M. Obaidat, V. Mohite, B. Issa, N. Tit, Y. Haik. Cryst. Res. Tech. **44**, *5*, 489 (2009). DOI: 10.1002/crat.200900022.
[87] L. Neel. J. Physique **15**, *4*, 225 (1954).
[88] A.S. Kamzin, L.A. Grigor'ev. JETP Lett. **57**, *9*, 557 (1993).
[89] A.S. Kamzin, L.A. Grigor'ev. ZETP **77**, *4*, 658 (1993).
[90] A.S. Kamzin, V.P. Rusakov, L.A. Grigoriev. Int. Conf. USSR. Proc. Part II, 271 (1988).
[91] A.S. Kamzin, L.A. Grigor'ev. Sov. Tech. Phys. Lett. **6**, *6*, 417 (1990).
[92] A.S. Kamzin, L.A. Grigor'ev. Sov. Tech. Phys. **35**, *7*, 840 (1990).
[93] F. Schaaf, U. Gonser. Hyperfine Interact. **57**, *1–4*, 2101 (1990).
[94] U. Gonzer, P. Schaaf, F. Aubertin. Hyperfine Interact. **66**, *1–4*, 95 (1991).
[95] A.S. Kamzin. JETP **89**, *5*, 891 (1999).
[96] A.S. Kamzin, L.P. Ol'khovik, V.L. Rozenbaum. Phys. Solid State **41**, *3*, 433 (1999).
[97] A.S. Kamzin, V.L. Rozenbaum, L.P. Ol'khovik. JETP Lett. **67**, *10*, 843 (1998).
[98] A.S. Kamzin, L.P. Olkhovik. FTT **41**, *10*, 1806 (1999). (in Russian).
[99] A.S. Kamzin, L.P. Ol'khovik, V.L. Rozenbaum. JETP **84**, *4*, 788 (1997).
[100] A.S. Kamzin, I.M. Obaidat, A.A. Valiullin, V.G. Semenov, I.A. Al-Omari. Phys. Solid State **62**, *10*, 1933 (2020). DOI: https://link.springer.com/article/10.1134/S1063783420100157
[101] M.E. Matsnev, V.S. Rusakov. AIP Conf. Proc. **1489**, *1*, 178 (2012).
[102] G.N. Konygin, O.M. Nemtsova, V.E. Porsev. Zhurn. prikl. spektroskopii **86**, *3*, 374 (2019). (in Russian).

Translated by A.Akhtyamov